LEARNING LOCAL EQUIVARIANT REPRESENTATIONS FOR QUANTUM OPERATORS

Anonymous authors
Paper under double-blind review

ABSTRACT

Predicting quantum operator matrices such as Hamiltonian, overlap, and density matrices in the density functional theory (DFT) framework is crucial for material science. Current methods often focus on individual operators and struggle with efficiency and scalability for large systems. Here we introduce a novel deep learning model, SLEM (strictly localized equivariant message-passing) for predicting multiple quantum operators, that achieves state-of-the-art accuracy while dramatically improving computational efficiency. SLEM's key innovation is its strict locality-based design for equivariant representations of quantum tensors while preserving physical symmetries. This enables complex many-body dependency without expanding the effective receptive field, leading to superior data efficiency and transferability. Using an innovative SO(2) convolution technique, SLEM reduces the computational complexity of high-order tensor products and is therefore capable of handling systems requiring the f and g orbitals in their basis sets. We demonstrate SLEM's capabilities across diverse 2D and 3D materials, achieving high accuracy even with limited training data. SLEM's design facilitates efficient parallelization, potentially extending DFT simulations to systems with device-level sizes, opening new possibilities for large-scale quantum simulations and high-throughput materials discovery.

1 INTRODUCTION

Quantum operators, representing observables and the evolution of quantum systems, are the cornerstone of describing the microscopic world. In modern quantum science, the advent of density functional theory (DFT) Hohenberg & Kohn (1964); Kohn & Sham (1965) has elevated single-particle quantum operators, such as the Kohn-Sham Hamiltonian, density matrix, and overlap matrix, to paramount importance in solving complex problems Jones (2015). These operators play a crucial role in unravelling electronic structures, predicting material properties, and advancing quantum technologies. However, as we tackle larger and more complex systems, these fundamental operators' efficient and accurate representation has emerged as a pressing challenge in computation, demanding new avenues for innovative methodologies.

Recent advances have incorporated machine learning (ML) techniques to accelerate DFT calculations by directly predicting DFT's output of quantum operators, including charge density Unke et al. (2021), overlapping matrix Yu et al. (2023); Unke et al. (2021), self-energy Dong et al. (2024), wave function Unke et al. (2021), and Hamiltonian matrix Yin et al. (2024); Yu et al. (2023); Gong et al. (2023); Nigam et al. (2022); Unke et al. (2021); Zhong et al. (2023). By circumventing self-consistent DFT calculations, such methods have the potential to scale up the electronic structure calculations. Some of the approaches utilize Gaussian regressions Nigam et al. (2022), kernel-based models Nigam et al. (2022), and neural networks Li et al. (2022) to predict invariant Hamiltonian matrix blocks on localized frames. Notably, powerful equivariant message-passing neural networks (E-MPNNs) have demonstrated remarkable accuracy Han et al. (2024); Musaelian et al. (2023); Batatia et al. (2022); Joshi et al. (2023); Liao & Smidt (2022); Liao et al. (2023); Simeon & De Fabritiis (2024); Passaro & Zitnick (2023); Zitnick et al. (2022). These networks ensure the output tensor blocks' equivariance, respecting atomic systems' physical priors. Typically, they use iterative updates to build many-body interactions, achieving high accuracy while enlarging the receptive field. This limits parallelization and, consequently, the model's scalability. The storage-intensive quantum

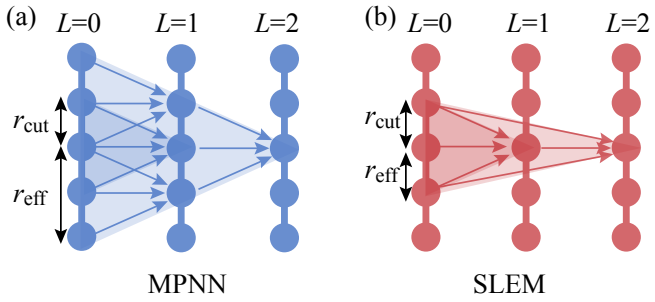

Figure 1: Local design of SLEM vs MPNN on 1D graph.(a) MPNN aggregation. (b) SLEM aggregation. Balls: nodes, sticks: edges, arrows: aggregation direction. r_{cut}: predefined cutoff; r_{eff}: effective cutoff after 2 layer updates. L: layer index.

tensor prediction tasks exacerbate these limitations, posing considerable challenges for training such models on large datasets or predicting quantum operators for extensive atomic structures .

Fortunately, the electrostatic screening counteracts the long-term dependency in a lot of material systems Huckel & Debye (1923); Resta (1977); Ninno et al. (2006). Therefore, quantum operators can be decomposed into elements dependent locally on atomic structures, which natrually prefers a strictly local model that avoids expanding the receptive field. The Allegro model Musaelian et al. (2023) applied this concept to build ML interatomic potentials (MLIPs), achieving high accuracy and parallelizability. While MLIPs only concern scalars (energy) and vectors (forces) (angular momentum $l = 0$ and 1) on each node, predicting quantum operators necessitates targeting both node and edge features on high-order spherical tensors (even up to $l = 6$ or 8). This requires locality and representability for both node and edge. Another significant challenge is computational complexity. To equivariantly mix the features of different angular momentum l, tensor products that scale as $\mathcal{O}(l^6)$ are required Passaro & Zitnick (2023). This makes model training, especially on heavy atoms, extremely slow. This limitation hinders the development of a unified ML DFT model that generalizes across the periodic table.

This work presents a novel method, the strictly localized equivariant message-passing model (SLEM), for efficient representations of quantum operators. SLEM employs a fully localized scheme to construct high-order node and edge equivariant features for a general representation of quantum operators, including the Hamiltonian and density matrix. As illustrated in Fig. 1, the model embeds localized edge hidden states and utilize them to construct localized node and edge features without including distant neighbours beyond a fixed cutoff range r_{cut}. This design enables the SLEM model to generalize better, parallelize easier, and scale to larger systems. Additionally, a fast and efficient SO(2) convolution Passaro & Zitnick (2023) is implemented to reduce the $\mathcal{O}(l^6)$ complexity, with edge-specific training weights, thereby further enhancing the model's accuracy. As for the overlap matrix, it is typically required for property calculations. Previous works have used another E-MPNN that doubles the network sizes Zhong et al. (2023) or extracts it from DFT calculations Gong et al. (2023); Yu et al. (2023), incurring additional costs or incorporating out-of-loop computation steps that complicate inference. In contrast, we utilized the two-centre integrals and parameterized the overlap matrix with spherical independent scalars (i.e., Slater-Koster (SK) parameters Slater & Koster (1954)). This method, inspired by the work of DeePTB Gu et al. (2023), fits the overlap operator representation with minimal additional cost.

2 Related Works

Message-passing Neural Networks Message-passing neural networks (MPNNs) Gilmer et al. (2017) have been widely applied in the modelling of atomic systems due to their exceptional accuracy in capturing the intricate relationships between atomic environments and physical properties Schütt et al. (2020). Previous works have predominantly utilized this scheme, achieving remarkably high precision in reported systems Schütt et al. (2018); Satorras et al. (2021); Han et al. (2024). However, as the MPNNs updates, the effective cutoff radius ($r_{\text{eff}} = N \times r_{\text{cut}}$) for each atom's features

grows linearly with the number of update steps (N), as shown in Fig. 1. Consequently, the effective neighbour list scales cubically with r_{eff}, making parallelization intractable. Allegro Musaelian et al. (2023) achieved locality modifies the updating rules by incorporating a hidden atom-pair state that depends partially on the centre atom. While this framework works successfully for scalars and l=1 vectors in potential energy prediction, it requires further improvement for fitting more general edge and node features. Other local methods avoid iterative updates that enlarge the receptive field, instead creating manually designed descriptors of the local environment Behler & Parrinello (2007); Bartók et al. (2010); Thompson et al. (2015); Zhang et al. (2018a); Wang et al. (2018); Zhang et al. (2018b). These methods are generally local, but often balance locality and representation capacity.

Equivariant Message Passing Physical quantities, under the law of nature, should be invariant or equivariant under the spatial and temporal symmetry operations. To model such quantities, a set of neural network models has been developed utilizing equivariant operations. Thomas et al. (2018); Weiler et al. (2018); Kondor et al. (2018); Kondor (2018) These neural networks possess physical priors to ensure outputs transform in sync with inputs, making them more generalizable, accurate, and data-efficient in predicting physical quantities. Formally, an equivariant operation from vector space X to Y is defined such that:

$$f(D_X[g]\mathbf{x}) = D_Y[g]f(\mathbf{x}) \quad \forall g \in G, \forall \mathbf{x} \in X$$

where $D_X[g] \in GL(X)$ is the representation of group element g on vector space X. Here we consider $O(3)$ group, then $\mathbf{x}, \mathbf{y}$ can be composed by irreducible representation (irreps for short) that are the spherical tensors with angular and magnetic momentum index l, m, and parity p such that $|m| \leq l$. Irreps with the same l support addition/subtraction, while a generalized multiplication is defined as tensor product ($\otimes$):

$$(\mathbf{x} \otimes \mathbf{y})^{l_3}_{m_3} = \sum_{m_1,m_2} C^{(l_3,m_3)}_{(l_1,m_1)(l_2,m_2)} \mathbf{x}^{l_1}_{m_1} \mathbf{y}^{l_2}_{m_2}$$

Where $C^{(l_3,m_3)}_{(l_1,m_2)(l_2,m_2)}$ are Clebsch-Gordan (CG) coefficients. Conventional tensor product has the time and memory scales of $O(l^6_{\text{max}})$ Passaro & Zitnick (2023) where l_{max} is the maximum angular momentum in $\mathbf{x}$ and $\mathbf{y}$. Such complexity poses great challenges for quantum tensor prediction. For example, constructing blocks of f-f and g-g orbital pairs require irreps of maximum order $l = 6$ and $l = 8$. Such high costs make training for large-size systems nearly impossible.

3 Model Architecure

3.1 Parameterize Equivariant Quantum Operators

The equivariant parameterization of quantum operators $\hat{O}$, such as the Hamiltonian and density matrix in the LCAO-based DFT framework, is illustrated in Fig. 2. The matrix element of operator $\hat{O}$ can be expressed as:

$$O^{i,j}_{l_1,l_2,m_1,m_2} = \langle i, l_1, m_1 | \hat{O} | j, l_2, m_2 \rangle \tag{1}$$

Here i and j denote atomic sites, while the angular and magnetic momentum index l, m label the atomic orbitals of the site. We apply the Wigner-Eckart theorem to decomposes the operator indexed by l_1, l_2 into a single index l_3 that satisfies $|l_1 - l_2| \leq l_3 \leq (l_1 + l_2)$:

$$o^{i,j}_{l_3,m_3} = \sum_{l_1,m_1,l_2,m_2} C^{(l_3,m_3)}_{(l_1,m_1)(l_2,m_2)} O^{i,j}_{l_1,l_2,m_1,m_2} \tag{2}$$

Here, the edge ($i \neq j$) and node ($i = j$) features $o^{i,j}_{l_3,m_3}$ are grouped by the index m into vectors of $\mathbf{o}^{i,j}_{c,l}$ with c accounting for multiple tensors for the same l. These features can be computed for hopping ($i \neq j$) and onsite ($i = j$) elements of the quantum operators. Further, by leveraging the Hermitian nature of quantum operators, the parameterized elements can be reduced to upper diagonal blocks. This is almost half the demanding storage. Then, we standardised $\mathbf{o}^{i,j}_{c,l}$ to balance the variance. Formally:

$$\mathbf{o}^{i,j}_{c,l} = \sigma^{Z_i,Z_j}_{c,l} \hat{\mathbf{o}}^{i,j}_{c,l} + \mu^{Z_i,Z_j}_{c,l} \delta_{l,0} \tag{3}$$

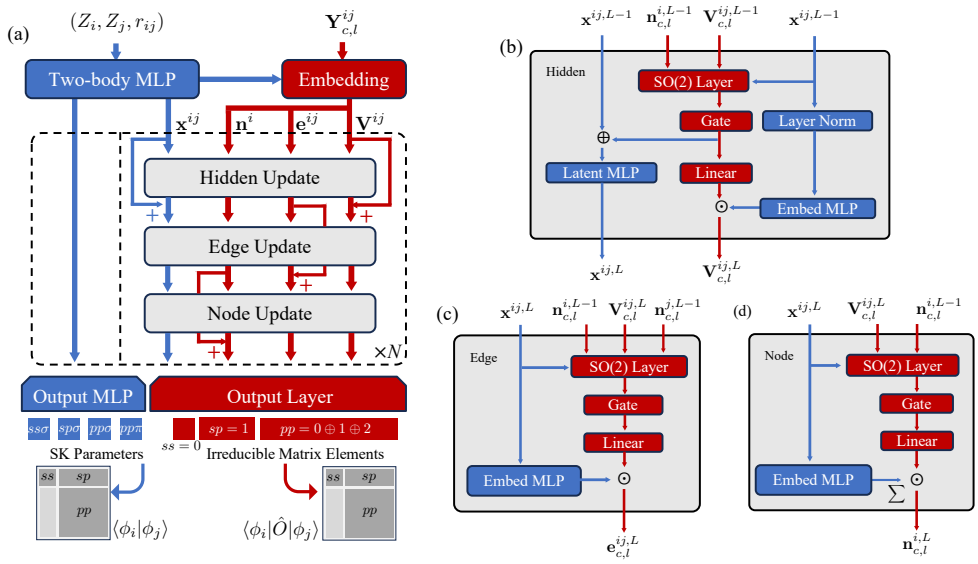

Figure 2: Design of the SLEM model. (a) Hierarchical structure of the model. Starts with the atomic number Z_i, the radial and spherical part of the shift vector $\boldsymbol{r}_{ij}$ and $\mathbf{Y}^{ij}_{c,l}$, the initialized hidden features $\mathbf{x}^{ij}$, $\mathbf{V}^{ij}$, along with edge and node features $\mathbf{e}^{ij}$, $\mathbf{n}^i$, are generated. The two-body hidden features predict the SK parameters constructing (off-)diagonal blocks for the overlap operator. Others features are then iteratively updated using the designed strictly localized updating scheme. (b)-(d) shows the hidden update (b), edge update (c), and node update (d). Node and edge features are used to construct the diagonal blocks for quantum operators.

Here, Z_i, Z_j are the atom species of atom i and j, $\sigma^{Z_i,Z_j}_{c,l}$ and $\mu^{Z_i,Z_j}_{c,l}$ are norm and bias value for each atom and atom-pair. These values are derived from the dataset statistics and applied as weights and biases in an atom/bond type-specific scaling layer. This step helps to resolve the unbalanced norms across diagonal and off-diagonal elements of quantum operators while facilitating using a ReLU-activated network to learn the normalized radial dependent decaying function from 1 to 0.

After supervising on the normalized features $\hat{\mathbf{o}}^{i,j}_{c,l}$, inverse transform from Eq. 2 is applied to reconstruct the predicted operator representations such as Hamiltonian and density matrix blocks:

$$O^{i,j}_{l_1,l_2,m_1,m_2} = \sum_{l_3,m_3} C^{(l_3,m_3)}_{(l_1,m_1)(l_2,m_2)} o^{i,j}_{l_3,m_3} \tag{4}$$

The whole procedure satisfies the rotational, transformational and reflectional symmetry.

3.2 Parameterize of Invariant Overlap Operators

The overlap matrix, analogous to other quantum operators, is defined as:

$$S^{i,j}_{l_1,l_2,m_1,m_2} = \langle i, l_1, m_1 | j, l_2, m_2 \rangle = \int \phi^{i,l_1}_{m_1}(\mathbf{r}) \phi^{j,l_2}_{m_2}(\mathbf{r} - \mathbf{r}_{ij}) d\mathbf{r} \tag{5}$$

where $\phi^{i,l}_m$ is the obital from LCAO bases. The overlap matrix also satisfies the equivariance relation. Since the equivariant dependency comes fully from the bases, it is possible to rotate them to align with the axis of $\mathbf{r}_{ij}$, reducing the angular dependence. Therefore, we can further simplify the matrix elements into scalars via the relation Podolskiy & Vogl (2004):

$$\int \phi^{i,l_1}_{m_1}(\mathbf{r}) \phi^{j,l_2}_{m_2}(\mathbf{r} - \mathbf{r}_{ij}) d\mathbf{r} = s^{Z_i,Z_j}_{l_1,l_2,|m_1|}(r_{ij}) \delta_{m_1,m_2} \tag{6}$$

Here, the dependency changes to Z_i, Z_j, and r_{ij}, indicating the two-center nature of the overlap integrals. Parameterizing these distance-dependent radial functions involves encoding atomic species

with radial information and a simple MLP to learn the mapping to target scalars.

$$f_{l_1,l_2,|m|}(Z_i, Z_j, r_{ij}) = s^{Z_i,Z_j}_{l_1,l_2,|m_1|}(r_{ij})\delta_{m_1,m_2} \tag{7}$$

After getting these parameters, we use them to construct the overlap matrix aligned with the bond axis, and then rotate it back to the original orientation.

3.3 THE SLEM MODEL

The SLEM model architecture is illustrated in Fig. 2. The model maintains a set of features, including hidden features $\mathbf{x}^{ij,L}, \mathbf{V}^{ij,L}_{c,l}$, node features $\mathbf{n}^{i,L}_{c,l}$ and edge features $\mathbf{e}^{ij,L}_{c,l}$ of hidden layer (L). Specifically, the hidden features consist of a scalar channel $\mathbf{x}^{ij,L}$ and a tensor channel $\mathbf{V}^{ij,L}_{c,l}$. The scalar channel is initialized as an embedded vector containing two-body information, including the atomic species and the radial distance of the atom pair. These initialized two-body radial features are then mapped by an MLP to the invariant SK parameters for overlap. For equivariant quantum operators, such as the Hamiltonian and density matrix, the scalar and tensor channels interact to generate an ordered atom-pair representations, which are used to construct local node and edge representations. After iterative updates, the representation is scaled by the statistical norm and biases, thereby achieving the final prediction.

3.3.1 FEATURE INITIALIZATION

Firstly, the initial scalar hidden feature is computed from the two-body embeddings of atomic species Z_i and Z_j, and the radial distance r_{ij}, as follows:

$$\mathbf{x}^{ij,L=0} = \mathbf{MLP}_{\text{2-body}}\left(\mathbf{1}(Z_i)||\mathbf{1}(Z_j)||\mathbf{B}(r_{ij})\right) \cdot u(r_{ij}) \tag{8}$$

Here, $||$ stands for vector concatenation, atom species are embedded with one-hot vectors denoted as $\mathbf{1}(Z)$, and a set of trainable Bessel bases $\mathbf{B}(r_{ij})$ is utilized to encode the distance r_{ij} between atoms i and j. $u(r_{ij})$ are envelope functions Batzner et al. (2022) to add explicit radial dependence. Subsequently, the edge and hidden features are initialized as weighted spherical harmonics of relative edge vectors:

$$\begin{aligned} \mathbf{V}^{ij,L=0}_{c,l} &= w_{c,l}\left(L_N\left(\mathbf{x}^{ij,L=0}\right)\right)\mathbf{Y}^{ij}_l \\ \mathbf{e}^{ij,L=0}_{c,l} &= w_{c,l}\left(\mathbf{x}^{ij,L=0}\right)\mathbf{Y}^{ij}_l \end{aligned} \tag{9}$$

Here, the weights are learned from the initialized scalar hidden features $\mathbf{x}^{ij,L=0}$. Layer normalization L_N ensures that the hidden tensor features have a balanced amplitude of each edge. The initial node features are then computed as linear transformations of the aggregated edge features:

$$\mathbf{n}^{i,L=0}_{c,l} = \mathbf{Linear}\left(\frac{1}{\sqrt{N_{\text{avg}}}}\sum_{j\in\mathcal{N}(i)}\mathbf{e}^{ij,L=0}_{c,l}\right) \tag{10}$$

Here $\mathcal{N}(i)$ and N_{avg} are the neighbouring atoms and the average number of neighbours of atom$-i$.

3.3.2 SPEED UP TENSOR PRODUCT

To integrate the information from the equivariant features, the tensor product is employed in all updating blocks of the SLEM model. Generally, the tensor product in SLEM is performed with the concatenated equivariant features $\tilde{\mathbf{f}}^{ij}_{c,l}$ and the weighted projection of the edge shift vector $\boldsymbol{r}_{ij} = \boldsymbol{r}_i - \boldsymbol{r}_j$ on the spherical harmonics function $\mathbf{Y}^{ij}_l$. Formally:

$$\mathbf{f}^{ij}_{c_3,l_3} = \tilde{\mathbf{f}}^{ij}_{c_1,l_1} \otimes w^{ij}_{c_2,l_2}\mathbf{Y}^{ij}_{l_2} = \sum_{c_1,l_1,l_2}\tilde{w}^{ij}_{c_1,l_1,l_2}\sum_{m_1,m_2}C^{(l_3,m_3)}_{(l_1,m_1)(l_2,m_2)}f^{ij}_{c_1,l_1,m_1}Y^{ij}_{l_2,m_2} \tag{11}$$

Here, $\tilde{w}^{ij}_{c_1,l_1,l_2} = \sum_{c_2} w_{c_1,c_2,l_1,l_2}w^{ij}_{c_2,l_2}$ are edge-specific parameters for each tensor product operation. Performing such tensor products on high-order features is computationally intensive. Therefore, we applied the recently developed SO(2) Passaro & Zitnick (2023) convolution to reduce the computation and storage complexity from $O(l^6_{\text{max}})$ to $O(l^3_{\text{max}})$ which we refer to the appendix.

3.3.3 HIDDEN UPDATES

To construct many-body interactions, as in Fig. 2(b), the node features $\mathbf{n}_{c,l}^{i}$ and hidden tensor features $\mathbf{V}_{c,l}^{ij}$ would be concatenated and doing tensor product with the projection coefficients of edge shift vector $\boldsymbol{r}_{ij}$ on the spherical harmonics functions. The operation is written formally as:

$$\tilde{\mathbf{V}}_{c_3,l_3}^{ij,L} = \left(\mathbf{n}^{i,L-1}||\mathbf{V}^{ij,L-1}\right)_{c_1,l_1} \otimes w_{c_2,l_2}^{ij,L}\mathbf{Y}_{l_2}^{ij} \tag{12}$$

Unlike most MPNN, the hidden states $\mathbf{x}^{ij}$ and $\mathbf{V}_{c,l}^{ij}$ in SLEM depend only on the local environment of centre atom i, the shift vector $\boldsymbol{r}_{ij}$, and the atomic type and coordinate informations of atom j. Such a design excludes neighbours of j into hidden states.

After the tensor production, the output features $\tilde{\mathbf{V}}_{c,l}^{ij,L}$ will be passed through the gated non-linearity Batzner et al. (2022), and transformed by an "E3linear" Geiger & Smidt (2022) layer to mix up the information across different channels. The new hidden feature will be multiplied by the weights learned from normalized scalar features to explicitly include the radial information and return as the updated feature $\mathbf{V}_{c,l}^{ij,L}$. The scalar hidden features are updated by mixing the 0th order information from $\mathbf{V}_{c,l}^{ij,L}$ with a latent MLP, which is:

$$\mathbf{x}^{ij,L} = \mathbf{MLP}\left(\mathbf{x}^{ij,L-1}||\mathbf{V}_{c,l=0}^{ij,L}\right) \cdot u(r_{ij}) \tag{13}$$

The scalar hidden states $\mathbf{x}^{ij,L}$ incorporate an explicit decaying envelope function $u(r_{ij})$ and many-body interactions of scalar and tensor features. This formulation effectively captures the decay behavior of each edge irrep feature as a function of radial distance.

3.3.4 NODE UPDATES

The strict local node representation $\mathbf{n}_{c,l}^{ij,L}$ can be constructed naturally from the many-body interactive tensor features $\mathbf{V}_{c,l}^{ij,L}$. We follow the MPNN style to create the message from node j to node i. Formally:

$$\mathbf{m}_{c_3,l_3}^{ij,L} = \left(\mathbf{n}^{i,L-1}||\mathbf{V}^{ij,L}\right)_{c_1,l_1} \otimes w_{c_2,l_2}^{ij,L}\mathbf{Y}_{l_2}^{ij} \tag{14}$$

Here again, we exclude the neighbouring information of atom j in $\mathbf{m}_{c_3,l_3}^{ij,L}$ via the partial updates of $\mathbf{V}_{c,l}^{ij,L}$, while maintaining necessary interactions. Each message then is passed through a gated activation and E3Linear layer, weighted separately by weights learnt from the hidden scalar features, and aggregated to update the node feature by:

$$\mathbf{n}_{c_3,l_3}^{ij,L} = \alpha \cdot \mathbf{n}_{c_3,l_3}^{ij,L-1} + \frac{\sqrt{1-\alpha^2}}{N_{avg}} \sum_{j \in \mathcal{N}(i)} w_{c_3,l_3}^{ij}\mathbf{m}_{c_3,l_3}^{ij,L} \tag{15}$$

Here α ranged from 0 to 1. The weights here differ from those in hidden updates as they are directly learnt from $\mathbf{x}^{ij,L}$ without normalization. Therefore, the absolute radial decay is enforced in the weights, providing a strong prior that the messages from atoms at shorter distances are generally more significant. Meanwhile, the update of $\mathbf{x}^{ij,L}$, and consequently w_{c_3,l_3}^{ij}, depends on the features $\mathbf{V}^{ij,L}$ and $\mathbf{n}^{i,L-1}$, as shown in Eq.13. This structure aligns with the equivariant graph attention mechanism Liao & Smidt (2022); Liao et al. (2023) which has demonstrated powerful expressibility in various tasks. Here w_{c_3,l_3}^{ij} corresponding to an attention score computed from $\mathbf{V}^{ij,L}$ and $\mathbf{n}^{i,L-1}$. Therefore, through this update, the dependencies of node features are strictly local.

3.3.5 EDGE UPDATES

The locality of edge features $\mathbf{e}_{c,l}^{ij,L}$ can be naturally preserved as long as the node features are strictly local. By mixing the information of node features on both sides, localized edge updates can be formulated as follows:

$$\tilde{\mathbf{e}}_{c_3,l_3}^{ij,L} = \left(\mathbf{n}^{i,L-1}||\mathbf{V}^{ij,L}||\mathbf{n}^{j,L-1}\right)_{c_1,l_1} \otimes w_{c_2,l_2}^{ij,L}\mathbf{Y}_{l_2}^{ij} \tag{16}$$

Table 1: MAE (in meV) for Hamiltonian matrix predictions using SLEM and other methods on materials with LCAO basis up to d orbitals. Numbers in parentheses indicate parameter count.

Systems with LCAO-basis up to d-orbitals					
Material	SLEM		DeepH-E3		HamGNN
	(0.7M)	(4.5M)	(1.0 M)	(4.5M)	(2.8M)
MoS_2	**0.34**	**0.14**	0.46	0.55	1.20
Graphene	**0.26**	**0.14**	0.40	0.28	0.35
Si(300K)	**0.10**	**0.07**	0.16	0.10	0.19

Table 2: MAE (in meV) for Hamiltonian matrix predictions using SLEM and DeepH-E3 models Gong et al. (2023) on materials with LCAO basis up to f and g orbitals. Numbers in parentheses indicate parameter count. The MAE of HfO_2 in DeepH-E3 is absent due to out-of-memory errors.

Systems with LCAO-basis up to f and g-orbitals		
Material	SLEM	DeepH-E3
	(1.7M)	(1.9M)
GaN	**0.21**	0.87
HfO_2	**0.28**	-

Similarly, the updated edge features are processed via a gated activation and an E3Linear layer, and then multiplied with weights learnt from the hidden scalar features (without normalization) as:

$$\mathbf{e}^{ij,L}_{c_3,l_3} = \alpha \cdot \mathbf{e}^{ij,L-1}_{c_3,l_3} + \sqrt{1-\alpha^2} \cdot w^{ij}_{c_3,l_3} \tilde{\mathbf{e}}^{ij,L}_{c_3,l_3} \tag{17}$$

The following section focuses on validating the effectiveness of this framework via learning equivariant DFT Hamiltonians, density matrices and overlap.

4 Results

4.1 Benchmark the accuracy and data-efficiency

We evaluate our model's performance in fitting Hamiltonian, density matrix, and overlap matrix using diverse datasets. For Hamiltonian, we use systems with up to d orbitals, including 2D systems of monolayer MoS_2 and graphene from existing datasets Li et al. (2022), as well as 3D bulk silicon generated for this study. To test SLEM's capability with high-order tensors, we also train the models on generated datasets of bulk GaN and HfO_2 systems, which include f and g orbitals. Structures in the Si, GaN, and HfO_2 systems are sampled via molecular dynamics using neural network potentials Wang et al. (2018). For density matrix and overlap matrix evaluations, we focus exclusively on the datasets of Si, GaN, and HfO_2 datasets, as the reported datasets for MoS_2 and graphene lack density and overlap matrix data.

Table 1 presents a comparison of mean absolute error (MAE) values in Hamiltonian prediction for graphene, MoS_2, and Si systems, whose LCAO basis extends up to d orbitals, among the SLEM, DeepH-E3 Gong et al. (2023), and HamGNN Zhong et al. (2023) methods. Our SLEM model achieves state-of-the-art accuracy, exhibiting the lowest MAE across all systems. Notably, this high accuracy is achieved with a relatively small model size of only 0.7 million (M) trainable parameters. Furthermore, we extended our comparison between the SLEM and DeepH-E3 methods to include GaN and HfO_2 systems, where the LCAO basis extends up to f and g orbitals, respectively. As shown in Table 2, the SLEM model consistently presents the lowest MAE, further demonstrating its high accuracy and versatility across different orbital complexities. Fig. 3 illustrates the band

Table 3: MAE for predicting density matrix using SLEM on materials with LCAO basis up to d, f, and g orbitals. Model settings align with those in Table 1.

SLEM density matrix model			
Materials	Silicon	GaN	HfO_2
MAE	8.9e-5	2.3e-5	3.9e-5

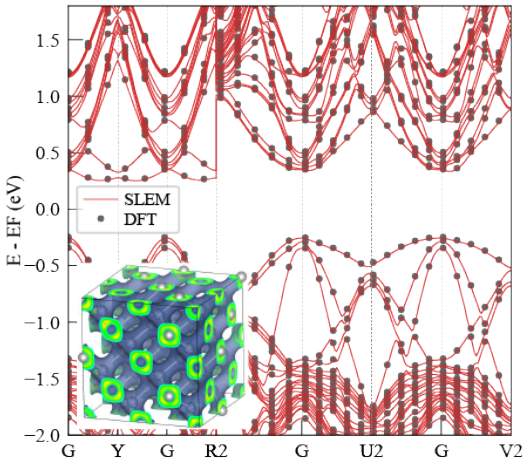

Figure 3: Comparison of band structures for a Si MD trajectory snapshot: SLEM prediction vs. DFT calculation. Predicted band structures are obtained from either diagonalization of the predicted Hamiltonian or NSCF DFT calculation using predicted charge density, yielding indistinguishable results. Inset: Visualization of charge density distribution for the same structure.

structure of silicon structures computed directly from the SLEM-predicted Hamiltonian, where the eigenvalues are indistinguishable from those obtained using DFT. For the density matrix, fitting results are presented in Table 3. The results demonstrate very high accuracy (order of 1e-5), approaching the machine precision limit of float32 numbers. In Fig. 3, we use the trained model to predict the density matrix and visualize its real-space distribution. This capability is particularly important for applications such as charge distribution analysis or tracking electron transfer. Furthermore, the predicted density can be directly used for non-self-consistent field (NSCF) DFT calculations. The resulting band structure for silicon, as an example, is highly accurate and matches the DFT output, with a MAE of only 1.09 meV in eigenvalues compared to self-consistent DFT results. The overlap matrix, represented by invariant SK parameters in our SLEM model, achieves exceptionally high accuracy as demonstrated in Table 4, approaching the machine precision limit for float32 numbers. Notably, our simplified parameterization enables this high accuracy with only a minimal increase in model complexity. For instance, in a silicon model designed to fit only the Hamiltonian, our typical parameter count is 0.7 M. The inclusion of overlap matrix prediction adds merely 0.01 M parameters, which is about 1.4% in total model size.

Additionally, the strict localization scheme of our SLEM model confers superior data efficiency, requiring fewer DFT-calculated data points for training. To quantify this efficiency, we conducted an experiment using randomly split subsets of the original data, comprising 20%, 40%, 60%, and 80% of the full training set. We trained both the SLEM model and DeepH-E3 method on these subsets and evaluated their performance on consistent validation sets. Results in table 5 demonstrate SLEM's high accuracy across all subsets, thus highlighting its remarkable data efficiency. This data efficiency implies that SLEM users can generate smaller, more cost-effective training sets. Moreover, SLEM's excellent data efficiency and transferability make it particularly well-suited as a backbone for developing universal DFT models, especially for systems involving heavy elements.

Table 4: MAE for predicting overlap matrix using SLEM's parameterization on materials with LCAO basis up to d, f, and g orbitals. Model settings align with those in Table 1.

SLEM overlap prediction			
Materials	Silicon	GaN	HfO_2
MAE	5.6e-5	4.7e-5	6.3e-5

Table 5: Comparison of validation MAE (in meV) for SLEM model and DeepH-E3 Gong et al. (2023) method trained on randomly split datasets Li et al. (2022) with varying training ratios. Model settings align with those in Table 1.

MoS2					
Partition	100%	80%	60%	40%	20%
SLEM	**0.34**	**0.37**	**0.39**	**0.37**	**0.37**
DeePH-E3	0.46	0.72	0.84	1.03	1.46
Graphene					
Partition	100%	80%	60%	40%	20%
SLEM	**0.26**	**0.26**	**0.27**	**0.21**	**0.26**
DeePH-E3	0.40	0.30	0.33	0.36	0.60

4.2 Efficiency and Scalability

In materials science, chemistry, and biology, many significant properties emerge in systems containing heavy atoms. These heavy atoms introduce high-order spherical tensors when representing quantum operators. Scaling to such systems is challenging due to the computational complexity of tensor products used to construct complex spherical tensors, which scales as $O(l^6)$. Conventional tensor production methods struggle with training and inference on systems containing heavy atoms, making it difficult to model these important phenomena efficiently. Moreover, inferring large material systems while training with small structures is particularly valuable, which requires parallelising the model inference by assigning partitions of the large atomic structure to multiple GPU workers. However, most current models struggle with this task. As the receptive fields expand through iterative graph updates, the minimum size of each partitioned subgraph increases, reducing the effectiveness of such partitioning. The SLEM model addresses these challenges by efficiently constructing high-order tensor products and assisting parallelization through its strict locality.

For efficiency, the implementation of SO(2) convolution reduces the tensor product computational complexity from $O(l^6)$ to $O(l^3)$, which is then further reduced by the parallelization of matrix operations to nearly $O(l)$ benefiting from PyTorch. Figure 4 compares the wall time and GPU memory consumed by tensor product operations using SO(2) convolution versus the conventional method employed in DeepH-E3 Gong et al. (2023) and E3NN Geiger & Smidt (2022). The SO(2) convolution approach demonstrates markedly superior efficiency, enabling our method to handle all possible basis choices in LCAO DFT. We also evaluated memory usage and training time for typical systems, comparing our model with DeepH-E3. The results, displayed in Fig. 5, show that our model consistently outperforms in both metrics. Notably, the advantage becomes more pronounced as the basis set size increases, highlighting our method's scalability. Additionally, the SLEM model's strict locality design significantly enhances parallelization. This localized approach allows for the division of the atomic graph into sub-graphs, enabling independent computation of node and edge features on separate devices. This is extremely important when expanding DFT simulation to large systems. In practice, for HfO_2 with $4s2p2d2f1g$ basis, a typical model of 1.7M parameters can predict the quantum operators for up to 10^3 atoms on devices with 32GB memory. Despite linear scaling, the inference on a system with $10^4 \sim 10^7$ would require over 300 GB of memory, necessitating parallelization across multiple GPUs. Therefore, a strictly localized model such as SLEM holds significant potential for expanding simulation system sizes.

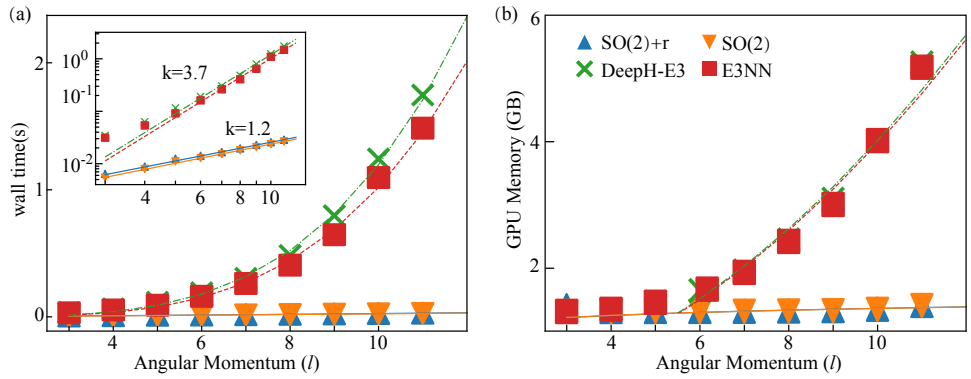

Figure 4: Comparison of time and memory consumption for different tensor-product implementations. (a) Time consumption vs. angular momentum (l) for different models, including the SO(2)-based SLEM model (triangles) with and without radial part (r), DeepH-E3 (cross) Gong et al. (2023), and E3NN (square) Geiger & Smidt (2022) models. Inset: Log-scale fit with slopes of 1.2 for the SLEM model and 3.7 for the other two models. (b) Memory consumption vs. l. The SLEM model demonstrates over two orders of magnitude improvement in both time and memory efficiency compared to DeepH-E3 and E3NN.

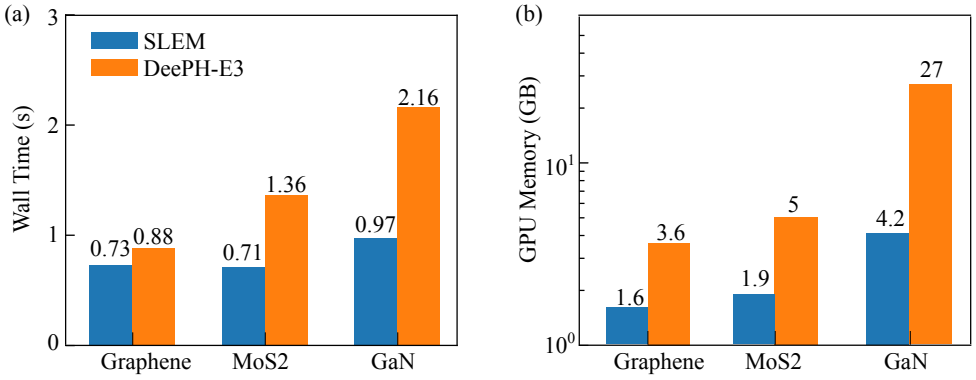

Figure 5: Comparison of training time per iteration and memory consumption with SLEM and DeepH-E3 Gong et al. (2023) models.

5 Conclusion

This work presents SLEM (Strictly Local Equivariant Message-passing) model, a novel approach for predicting quantum operator representations in materials science. By employing a strict locality design and integrating SO(2) convolution, SLEM achieves state-of-the-art performance in predicting Hamiltonians, density matrices, and overlap matrices for diverse materials, including systems with heavy atoms. The model's efficiency and scalability open new possibilities for large-scale quantum simulations and high-throughput materials discovery. Notably, SLEM's locality enables efficient parallelization through atomic graph partitioning, potentially extending its applicability to extremely large systems at device-level scales. SLEM's intrinsic support for multiple quantum operators, coupled with its novel overlap matrix parameterization, significantly reduces computational costs and dependence on post-training DFT software. The model demonstrates superior data efficiency and transferability, making it particularly well-suited for developing universal DFT models, especially for systems involving heavy elements. These advancements position SLEM as a powerful tool for simulating complex systems in materials science and computational chemistry. Looking ahead, future work will focus on developing robust sampling methodologies for active learning and integrating SLEM with existing software ecosystems to fully leverage its capabilities in real-world applications, further advancing the field of computational materials science.

REFERENCES

Albert P. Bartók, Mike C. Payne, Risi Kondor, and Gábor Csányi. Gaussian approximation potentials: The accuracy of quantum mechanics, without the electrons. *Phys. Rev. Lett.*, 104:136403, Apr 2010. doi: 10.1103/PhysRevLett.104.136403. URL https://link.aps.org/doi/10.1103/PhysRevLett.104.136403.

Ilyes Batatia, David P Kovacs, Gregor Simm, Christoph Ortner, and Gábor Csányi. MACE: Higher order equivariant message passing neural networks for fast and accurate force fields. *Advances in Neural Information Processing Systems*, 35:11423–11436, 2022. URL https://proceedings.neurips.cc/paper_files/paper/2022/file/4a36c3c51af11ed9f34615b81edb5bbc-Paper-Conference.pdf.

Simon Batzner, Albert Musaelian, Lixin Sun, Mario Geiger, Jonathan P Mailoa, Mordechai Kornbluth, Nicola Molinari, Tess E Smidt, and Boris Kozinsky. E(3)-equivariant graph neural networks for data-efficient and accurate interatomic potentials. *Nature Communications*, 13(1):2453, 2022. URL https://doi.org/10.1038/s41467-022-29939-5.

Jörg Behler and Michele Parrinello. Generalized neural-network representation of high-dimensional potential-energy surfaces. *Phys. Rev. Lett.*, 98:146401, Apr 2007. doi: 10.1103/PhysRevLett.98.146401. URL https://link.aps.org/doi/10.1103/PhysRevLett.98.146401.

Xinyang Dong, Emanuel Gull, and Lei Wang. Equivariant neural network for green's functions of molecules and materials. *Phys. Rev. B*, 109:075112, Feb 2024. doi: 10.1103/PhysRevB.109.075112. URL https://link.aps.org/doi/10.1103/PhysRevB.109.075112.

Mario Geiger and Tess Smidt. e3nn: Euclidean neural networks. *arXiv:2207.09453*, 2022. URL https://arxiv.org/abs/2207.09453.

Justin Gilmer, Samuel S Schoenholz, Patrick F Riley, Oriol Vinyals, and George E Dahl. Neural message passing for quantum chemistry. In *International conference on machine learning*, pp. 1263–1272. PMLR, 2017. URL https://dl.acm.org/doi/10.5555/3305381.3305512.

Xiaoxun Gong, He Li, Nianlong Zou, Runzhang Xu, Wenhui Duan, and Yong Xu. General framework for E(3)-equivariant neural network representation of density functional theory Hamiltonian. *Nature Communications*, 14(1):2848, 2023. URL https://doi.org/10.1038/s41467-023-38468-8.

Qiangqiang Gu, Zhanghao Zhouyin, Shishir Kumar Pandey, Peng Zhang, Linfeng Zhang, and Weinan E. DeePTB: A deep learning-based tight-binding approach with $ab\ initio$ accuracy. *arXiv:2307.04638*, 2023. URL https://arxiv.org/abs/2307.04638.

Jiaqi Han, Jiacheng Cen, Liming Wu, Zongzhao Li, Xiangzhe Kong, Rui Jiao, Ziyang Yu, Tingyang Xu, Fandi Wu, Zihe Wang, et al. A survey of geometric graph neural networks: Data structures, models and applications. *arXiv:2403.00485*, 2024. URL https://arxiv.org/abs/2403.00485.

P. Hohenberg and W. Kohn. Inhomogeneous electron gas. *Phys. Rev.*, 136:B864–B871, Nov 1964. doi: 10.1103/PhysRev.136.B864. URL https://link.aps.org/doi/10.1103/PhysRev.136.B864.

E Huckel and P Debye. Zur theorie der elektrolyte. i. gefrierpunktserniedrigung und verwandte erscheinungen. *Phys. Z*, 24:185–206, 1923.

Simão M João, Miša Anelković, Lucian Covaci, Tatiana G Rappoport, João MVP Lopes, and Aires Ferreira. Kite: high-performance accurate modelling of electronic structure and response functions of large molecules, disordered crystals and heterostructures. *Royal Society Open Science*, 7(2):191809, 2020. URL https://royalsocietypublishing.org/doi/abs/10.1098/rsos.191809.

R. O. Jones. Density functional theory: Its origins, rise to prominence, and future. *Rev. Mod. Phys.*, 87:897–923, Aug 2015. doi: 10.1103/RevModPhys.87.897. URL https://link.aps.org/doi/10.1103/RevModPhys.87.897.

Chaitanya K Joshi, Cristian Bodnar, Simon V Mathis, Taco Cohen, and Pietro Lio. On the expressive power of geometric graph neural networks. In *International conference on machine learning*, pp. 15330–15355. PMLR, 2023. URL https://proceedings.mlr.press/v202/joshi23a/joshi23a.pdf.

W. Kohn and L. J. Sham. Self-consistent equations including exchange and correlation effects. *Phys. Rev.*, 140:A1133–A1138, Nov 1965. doi: 10.1103/PhysRev.140.A1133. URL https://link.aps.org/doi/10.1103/PhysRev.140.A1133.

Risi Kondor. N-body networks: a covariant hierarchical neural network architecture for learning atomic potentials. *arXiv:1803.01588*, 2018. URL https://arxiv.org/abs/1803.01588.

Risi Kondor, Zhen Lin, and Shubhendu Trivedi. Clebsch–Gordan nets: a fully fourier space spherical convolutional neural network. *Advances in Neural Information Processing Systems*, 31, 2018. URL https://proceedings.neurips.cc/paper_files/paper/2018/file/a3fc981af450752046be179185ebc8b5-Paper.pdf.

He Li, Zun Wang, Nianlong Zou, Meng Ye, Runzhang Xu, Xiaoxun Gong, Wenhui Duan, and Yong Xu. Deep-learning density functional theory hamiltonian for efficient ab initio electronic-structure calculation. *Nature Computational Science*, 2(6):367–377, 2022. URL https://doi.org/10.1038/s43588-022-00265-6.

Yunhai Li, Zhen Zhan, Xueheng Kuang, Yonggang Li, and Shengjun Yuan. TBPLaS: A tight-binding package for large-scale simulation. *Computer Physics Communications*, 285:108632, April 2023. ISSN 0010-4655. doi: 10.1016/j.cpc.2022.108632.

Yi-Lun Liao and Tess Smidt. Equiformer: Equivariant graph attention transformer for 3d atomistic graphs. *arXiv:2206.11990*, 2022. URL https://arxiv.org/abs/2206.11990.

Yi-Lun Liao, Brandon Wood, Abhishek Das, and Tess Smidt. Equiformerv2: Improved equivariant transformer for scaling to higher-degree representations. *arXiv:2306.12059*, 2023. URL https://arxiv.org/abs/2306.12059.

Albert Musaelian, Simon Batzner, Anders Johansson, Lixin Sun, Cameron J. Owen, Mordechai Kornbluth, and Boris Kozinsky. Learning local equivariant representations for large-scale atomistic dynamics. *Nature Communications*, 14(1):579, February 2023. ISSN 2041-1723. doi: 10.1038/s41467-023-36329-y.

Jigyasa Nigam, Michael J. Willatt, and Michele Ceriotti. Equivariant representations for molecular Hamiltonians and N-center atomic-scale properties. *The Journal of Chemical Physics*, 156(1): 014115, 01 2022. ISSN 0021-9606. doi: 10.1063/5.0072784. URL https://doi.org/10.1063/5.0072784.

D. Ninno, F. Trani, G. Cantele, K. J. Hameeuw, G. Iadonisi, E. Degoli, and S. Ossicini. Thomas-Fermi model of electronic screening in semiconductor nanocrystals. *Europhysics Letters*, 74(3): 519, mar 2006. doi: 10.1209/epl/i2005-10544-9. URL https://dx.doi.org/10.1209/epl/i2005-10544-9.

Saro Passaro and C Lawrence Zitnick. Reducing SO(3) convolutions to SO(2) for efficient equivariant gnns. In *International Conference on Machine Learning*, pp. 27420–27438. PMLR, 2023. URL https://dl.acm.org/doi/10.5555/3618408.3619548.

A. V. Podolskiy and P. Vogl. Compact expression for the angular dependence of tight-binding Hamiltonian matrix elements. *Phys. Rev. B*, 69:233101, Jun 2004. doi: 10.1103/PhysRevB.69.233101. URL https://link.aps.org/doi/10.1103/PhysRevB.69.233101.

Raffaele Resta. Thomas-fermi dielectric screening in semiconductors. *Phys. Rev. B*, 16:2717–2722, Sep 1977. doi: 10.1103/PhysRevB.16.2717. URL https://link.aps.org/doi/10.1103/PhysRevB.16.2717.

Vıctor Garcia Satorras, Emiel Hoogeboom, and Max Welling. E(n) equivariant graph neural networks. In *International conference on machine learning*, pp. 9323–9332. PMLR, 2021. URL https://proceedings.mlr.press/v139/satorras21a/satorras21a.pdf.

K. T. Schütt, H. E. Sauceda, P.-J. Kindermans, A. Tkatchenko, and K.-R. Müller. SchNet – A deep learning architecture for molecules and materials. *The Journal of Chemical Physics*, 148(24): 241722, 03 2018. ISSN 0021-9606. doi: 10.1063/1.5019779. URL https://doi.org/10.1063/1.5019779.

Kristof T Schütt, Stefan Chmiela, O Anatole Von Lilienfeld, Alexandre Tkatchenko, Koji Tsuda, and Klaus-Robert Müller. Machine learning meets quantum physics. *Lecture Notes in Physics*, 2020.

Guillem Simeon and Gianni De Fabritiis. TensorNet: Cartesian tensor representations for efficient learning of molecular potentials. *Advances in Neural Information Processing Systems*, 36, 2024. URL https://openreview.net/forum?id=BEHlPdBZ2e.

J. C. Slater and G. F. Koster. Simplified LCAO method for the periodic potential problem. *Phys. Rev.*, 94:1498–1524, Jun 1954. doi: 10.1103/PhysRev.94.1498. URL https://link.aps.org/doi/10.1103/PhysRev.94.1498.

Nathaniel Thomas, Tess Smidt, Steven Kearnes, Lusann Yang, Li Li, Kai Kohlhoff, and Patrick Riley. Tensor field networks: Rotation-and translation-equivariant neural networks for 3d point clouds. *arXiv:1802.08219*, 2018. URL https://arxiv.org/abs/1802.08219.

A.P. Thompson, L.P. Swiler, C.R. Trott, S.M. Foiles, and G.J. Tucker. Spectral neighbor analysis method for automated generation of quantum-accurate interatomic potentials. *Journal of Computational Physics*, 285:316–330, 2015. ISSN 0021-9991. doi: https://doi.org/10.1016/j.jcp.2014.12.018. URL https://www.sciencedirect.com/science/article/pii/S0021999114008353.

Oliver Unke, Mihail Bogojeski, Michael Gastegger, Mario Geiger, Tess Smidt, and Klaus-Robert Müller. SE(3)-equivariant prediction of molecular wavefunctions and electronic densities. *Advances in Neural Information Processing Systems*, 34:14434–14447, 2021. URL https://proceedings.neurips.cc/paper/2021/file/78f1893678afbeaa90b1fa01b9cfb860-Paper.pdf.

Jonathan Vandermause, Steven B. Torrisi, Simon Batzner, Yu Xie, Lixin Sun, Alexie M. Kolpak, and Boris Kozinsky. On-the-fly active learning of interpretable Bayesian force fields for atomistic rare events. *npj Computational Materials*, 6(1):1–11, March 2020. ISSN 2057-3960. doi: 10.1038/s41524-020-0283-z.

Han Wang, Linfeng Zhang, Jiequn Han, and Weinan E. DeePMD-kit: A deep learning package for many-body potential energy representation and molecular dynamics. *Computer Physics Communications*, 228:178–184, July 2018. ISSN 0010-4655. doi: 10.1016/j.cpc.2018.03.016.

Maurice Weiler, Mario Geiger, Max Welling, Wouter Boomsma, and Taco S Cohen. 3D Steerable CNNs: Learning rotationally equivariant features in volumetric data. *Advances in Neural Information Processing Systems*, 31, 2018. URL https://proceedings.neurips.cc/paper_files/paper/2018/file/488e4104520c6aab692863cc1dba45af-Paper.pdf.

Shi Yin, Xinyang Pan, Fengyan Wang, Feng Wu, and Lixin He. A framework of so(3)-equivariant non-linear representation learning and its application to electronic-structure hamiltonian prediction. *arXiv:2405.05722*, 2024. URL https://arxiv.org/abs/2405.05722.

Haiyang Yu, Zhao Xu, Xiaofeng Qian, Xiaoning Qian, and Shuiwang Ji. Efficient and equivariant graph networks for predicting quantum hamiltonian. In *International Conference on Machine Learning*, pp. 40412–40424. PMLR, 2023. URL https://proceedings.mlr.press/v202/yu23i.html.

Linfeng Zhang, Jiequn Han, Han Wang, Roberto Car, and Weinan E. Deep potential molecular dynamics: A scalable model with the accuracy of quantum mechanics. *Phys. Rev. Lett.*, 120:143001, Apr 2018a. doi: 10.1103/PhysRevLett.120.143001. URL https://link.aps.org/doi/10.1103/PhysRevLett.120.143001.

Linfeng Zhang, Jiequn Han, Han Wang, Wissam Saidi, Roberto Car, and Weinan E. End-to-end symmetry preserving inter-atomic potential energy model for finite and extended systems. *Advances in Neural Information Processing Systems*, 31, 2018b. URL https://proceedings.neurips.cc/paper_files/paper/2018/file/e2ad76f2326fbc6b56a45a56c59fafdb-Paper.pdf.

Yuzhi Zhang, Haidi Wang, Weijie Chen, Jinzhe Zeng, Linfeng Zhang, Han Wang, and Weinan E. DP-GEN: A concurrent learning platform for the generation of reliable deep learning based potential energy models. *Computer Physics Communications*, 253:107206, 2020. ISSN 0010-4655. doi: https://doi.org/10.1016/j.cpc.2020.107206. URL https://www.sciencedirect.com/science/article/pii/S001046552030045X.

Yang Zhong, Hongyu Yu, Mao Su, Xingao Gong, and Hongjun Xiang. Transferable equivariant graph neural networks for the hamiltonians of molecules and solids. *npj Computational Materials*, 9(1):182, 2023. URL https://doi.org/10.1038/s41524-023-01130-4.

Larry Zitnick, Abhishek Das, Adeesh Kolluru, Janice Lan, Muhammed Shuaibi, Anuroop Sriram, Zachary Ulissi, and Brandon Wood. Spherical channels for modeling atomic interactions. *Advances in Neural Information Processing Systems*, 35:8054–8067, 2022. URL https://proceedings.neurips.cc/paper_files/paper/2022/file/3501bea1ac61fedbaaff2f88e5fa9447-Paper-Conference.pdf.

A Comparison of SLEM with MPNN

Message-passing Neural Networks In the message-passing scheme, atoms are treated as nodes in graphs, with bonds to neighbouring atoms represented as connected edges within a specified cutoff radius. The embedded atomic features are processed by trainable functions, generating messages from each edge to update the embeddings of central atoms. Formally, the MPNN framework can be summarized as follows:

$$\begin{aligned}\mathbf{e}^{ij,L} &= \mathcal{N}_L\left(\mathbf{n}^{i,L-1}, \mathbf{n}^{j,L-1}, \mathbf{e}^{ij,L-1}\right)\\ \mathbf{m}^{ij,L} &= M_L\left(\mathbf{n}^{i,L-1}, \mathbf{n}^{j,L-1}, \mathbf{e}^{ij,L}\right)\\ \mathbf{n}^{i,L} &= U_L\left(\mathbf{n}^{i,L-1}, \sum_{j\in\mathcal{N}(i)} \mathbf{m}^{ij,L}\right)\end{aligned}$$

Here, $\mathbf{e}^{ij,L}$ represents the edge features, $\mathbf{m}^{ij,L}$ denotes the messages, and $\mathbf{n}^{i,L}$ indicates the node features at layer L. $\mathcal{N}_L$, M_L, and U_L are the trainable functions for the edge, message, and node updates. $\mathcal{N}(i) = \{j | r_{ij} < r_{\text{cut}}\}$ indicates all the neighbour atoms for atom i, with r_{cut} being the predefined cutoff. This updating framework allows for the construction of many-body interactions and long-term dependencies, leading to strong performance across various applications. Here we reframe the updating rules of SLEM with the MPNN framework, which looks like this:

$$\begin{aligned}\mathbf{V}^{ij,L} &= \mathcal{V}_L\left(\mathbf{n}^{i,L-1}, \mathbf{V}^{ij,L-1}\right)\\ \mathbf{e}^{ij,L} &= \mathcal{N}_L\left(\mathbf{n}^{i,L-1}, \mathbf{V}^{ij,L}, \mathbf{n}^{j,L-1}, \mathbf{e}^{ij,L-1}\right)\\ \mathbf{m}^{ij,L} &= M_L\left(\mathbf{n}^{i,L-1}, \mathbf{V}^{ij,L}\right)\\ \mathbf{n}^{i,L} &= U_L\left(\mathbf{n}^{i,L-1}, \sum_{j\in\mathcal{N}(i)} \mathbf{m}^{ij,L}\right)\end{aligned}$$

Here $\mathcal{V}_L$ is the neural network for hidden feature construction. This update scheme constructs many-body interactions to build equivariant edge and node features while preserving the absolute locality by excluding atoms outside the constant cutoff radius. Such a scheme, in principle, would have much better transferability, data efficiency, as well as scalability when we have a strong prior that the input and output are dependent spatially local.

B MORE ON TENSOR PRODUCT

To integrate the information from the equivariant features, the tensor product is employed in all updating blocks of the SLEM model. Generally, the tensor product in SLEM is performed with the concatenated equivariant features $\tilde{\mathbf{f}}_{c,l}^{ij}$ and the weighted projection of the edge shift vector $\boldsymbol{r}_{ij} = \boldsymbol{r}_i - \boldsymbol{r}_j$ on the spherical harmonics function $\mathbf{Y}_l^{ij}$. Formally:

$$\mathbf{f}_{c_3,l_3}^{ij} = \tilde{\mathbf{f}}_{c_1,l_1}^{ij} \otimes w_{c_2,l_2}^{ij} \mathbf{Y}_{l_2}^{ij} = \sum_{c_1,l_1,l_2} \tilde{w}_{c_1,l_1,l_2}^{ij} \sum_{m_1,m_2} C_{(l_1,m_1)(l_2,m_2)}^{(l_3,m_3)} f_{c_1,l_1,m_1}^{ij} Y_{l_2,m_2}^{ij} \tag{18}$$

Here, $\tilde{w}_{c_1,l_1,l_2}^{ij} = \sum_{c_2} w_{c_1,c_2,l_1,l_2} w_{c_2,l_2}^{ij}$ are edge-specific parameters for each tensor product operation. Performing such tensor products on high-order features is computationally intensive. Therefore, we applied the recently developed SO(2) Passaro & Zitnick (2023) convolution to simplify, reducing the computation and storage complexity from $O(l_{\text{max}}^6)$ to $O(l_{\text{max}}^3)$. The simplification idea is intuitive. $\mathbf{Y}_{l_2,m_2}^{ij}$ are sparse tensors if rotated to align with the edge ij, which is nonzero only for $m_2 = 0$. Therefore, it is easier to compute the tensor production in the direction of edge ij, and rotate inversely the output afterwards. This step removes the m_2 index from the summation in Eq. 18. Furthermore, considering the Clebsch-Gordan coefficients with $m_2 = 0$, we find that $C_{(l_1,m_1)(l_2,0)}^{(l_3,m_3)} = 0$ except for $m_3 = \pm m_1$. This allows further reduction of the summation in Eq. 18 by replacing $\pm m_1$ with a single index m. Then the operations can be reformulated formally as:

$$\begin{pmatrix} f_{c,l,m}^{ij} \\ f_{c,l,-m}^{ij} \end{pmatrix} = \sum_{c',l'} \begin{pmatrix} w_{c,c',l',m} & -w_{c,c',l',-m} \\ w_{c,c',l',-m} & w_{c,c',l',m} \end{pmatrix} \cdot \begin{pmatrix} \tilde{f}_{c',l',m}^{ij} \\ \tilde{f}_{c',l',-m}^{ij} \end{pmatrix}$$

This represents a linear operation on $\tilde{f}_{c',l',m'}^{ij}$. By employing this method, high-order tensor products for $l = 8$, 9 and even 10 can be efficiently calculated, which is essential for heavy element systems where the f, g or even higher orbitals are used in the LCAO basis for DFT calculations. Finally, the weights for the new SO(2) tensor product method are multiplied by edge-specific parameters, where $w_{c',l'}^{ij}$ are mapped by an MLP from hidden scalar features $\mathbf{x}^{ij,L}$ as $\tilde{w}_{c,c',l',m}^{ij} = w_{c,c',l',m} w_{c',l'}^{ij}$. This powerful and efficient tensor product layer facilitates the construction of local interactive updates of the features.

C LIMITATION

The SLEM model, benefiting from the Strictly localized design, performs better in accuracy and transferability as demonstrated in various datasets. We acknowledge that such a localized hypothesis is most suitable for describing periodic systems, which is commonly adopted in physics, chemistry and material science research. For confined systems such as molecules, the absence of screening effect could lead to long-term dependency that is uncovered within prefixed cutoff. In these cases, the SLEM model wouldn't perform as well as in periodic cases. For generality, we also proposed a semilocal model called LEM (Localized Equivarient Message-Passing), where the interaction between distant atoms is included but decays exponentially with their distance, with a trainable decay factor. All the designed models are ready to use in our GitHub repository.

D FUTURE INVESTIGATION

While SLEM demonstrates efficacy across various applications, several areas warrant further investigation:

- Sampling Methodology for Active Learning: Scientific computation tasks require high confidence in calculated results, which can be challenging for data-driven approaches. Developing a robust sampling workflow for active learning is essential for reliability. While techniques like uncertainty-driven sampling with Gaussian regression Vandermause et al. (2020) or model ensembles Zhang et al. (2020) have addressed confidence issues in machine learning force fields, designing a sampling workflow specifically for quantum operator models remains an open question.

- Software Integration for Post-Processing: Integrating the model with existing software is vital, especially for high-throughput calculations and large atomic systems beyond conventional DFT capabilities. An efficient, parallelizable solver for extracting physical quantities from the model's predictions is highly beneficial. While some software based on stochastic techniques Li et al. (2023); João et al. (2020) shows promise, an open-sourced and highly-optimized solution for non-orthogonal bases remains unavailable.

Future research addressing these challenges will further enhance the applicability and reliability of SLEM and similar quantum operator models in computational materials science and chemistry.